Extreme Mechanics Letters 9 (2016) 269–281

Contents lists available at ScienceDirect

Extreme Mechanics Letters

journal homepage: www.elsevier.com/locate/eml

Recent progress in flexible and stretchable piezoelectric devices for mechanical energy harvesting, sensing and actuation

Canan Dagdeviren [a,b], Pauline Joe [b], Ozlem L. Tuzman [c], Kwi-Il Park [d], Keon Jae Lee [e], Yan Shi [f,g], Yonggang Huang [h,i,j,k], John A. Rogers [l,m,n,o,p,*]

[a] Harvard Society of Fellows, Harvard University, Cambridge, MA 02138, USA

[b] The David H. Koch Institute for Integrative Cancer Research, Massachusetts Institute of Technology, Cambridge, MA 02139, USA

[c] Robert College, Istanbul, 34345, Turkey

[d] Department of Energy Engineering, Gyeongnam National University of Science and Technology (GNTECH), Jinju-si, 52725, Republic of Korea

[e] Department of Materials Science and Engineering, Korea Advanced Institute of Science and Technology (KAIST), Daejeon, 34141, Republic of Korea

[f] Center for Mechanics and Materials, Department of Engineering Mechanics, Tsinghua University, Beijing 100084, China

[g] AML, Department of Engineering Mechanics, Tsinghua University, Beijing 100084, China

[h] Department of Civil and Environmental Engineering, Northwestern University, Evanston, IL 60208, USA

[i] Department of Mechanical Engineering, Northwestern University, Evanston, IL 60208, USA

[j] Center for Engineering and Health, Northwestern University, Evanston, IL 60208, USA

[k] Skin Disease Research Center, Northwestern University, Evanston, IL 60208, USA

[l] Department of Materials Science and Engineering, Beckman Institute for Advanced Science and Technology, University of Illinois at Urbana-Champaign, Urbana, IL 61801, USA

[m] Frederick Seitz Materials Research Laboratory, University of Illinois at Urbana-Champaign, Urbana, IL 61801, USA

[n] Department of Chemistry, University of Illinois at Urbana-Champaign, Urbana, IL 61801, USA

[o] Department of Mechanical Science and Engineering, University of Illinois at Urbana-Champaign, Urbana, IL 61801, USA

[p] Department of Electrical and Computer Engineering, University of Illinois at Urbana-Champaign, Urbana, IL 61801, USA

ARTICLE INFO

Article history:
Received 3 May 2016
Accepted 28 May 2016
Available online 11 June 2016

Keywords:
Piezoelectrics
Buckling
Elastomers
Flexible electronics
Stretchable electronics
Bio-integrated electronics

ABSTRACT

Recent advances in materials science and mechanical engineering enable the realization of high performance piezoelectric systems in soft, flexible/stretchable formats, with unique opportunities for use in bio-integrated applications, from mechanical energy harvesting to sensing and actuation. This article highlights the essential mechanical to electrical conversion processes in devices and systems of this type, along with key considerations in their designs. Quantitative, experimentally validated mechanics models provide guidelines in the selection of optimized configurations and materials choices. The former focuses on thin geometries, neutral mechanical plane construction and controlled buckling. The latter includes options such as organic polymers, inorganic nanomaterials and various types of composites. Concluding sections summarize representative applications in biomedicine, ranging from devices for mechanical energy harvesting from natural motions of internal organs to sensors and actuators for the skin.

* Corresponding author at: Department of Materials Science and Engineering, Beckman Institute for Advanced Science and Technology, University of Illinois at Urbana-Champaign, Urbana, IL 61801, USA.
E-mail address: jrogers@illinois.edu (J.A. Rogers).

http://dx.doi.org/10.1016/j.eml.2016.05.015
2352-4316/

Contents

1. Introduction 270
2. Discussion 270
2.1. Coupled mechanical and electrical behaviors in flexible piezoelectric systems 270
2.2. Inorganic piezoelectric materials 273
2.3. Organic and composite piezoelectric materials 274
2.4. Inorganic piezoelectric devices in biomedicine 276
3. Conclusion and outlook 280
References 280

1. Introduction

Recent developments in materials science, mechanics and manufacturing now enable the construction of piezoelectric devices in formats that are thin, flexible and, in some cases, mechanically stretchable. The results allow straightforward miniaturization of lightweight, compliant electromechanical systems suitable for mounting on nearly any type of surface, with performance characteristics that can match those of conventional, rigid devices. Such technologies leverage the ability of piezoelectric materials to interconvert mechanical and electrical forms of energy [1]. Electrical power can be generated from vibrations associated with operating machinery, movements of the human body and environmental sources, such as waves, wind, and others. Similarly, application of electric fields to piezoelectric materials yields well-controlled mechanical forces for actuation in robotics, biomedical devices and metrology tools. These dual functions in piezoelectrics, together with an increasingly broad set of material choices [2–12] and device designs, provide the foundations for numerous applications [13–15] of growing interest, particularly in wearable or implantable systems. Here, recent capabilities in rendering piezoelectric devices in thin, mechanically 'soft' formats are critically important. Specific examples include sustainable power sources in consumer electronics [13] and sensors for blood pressure measurements [16].

Various options can be considered for the use of piezoelectric materials in such contexts. Established strategies to deploy the highest performance, inorganic piezoelectric materials rely on methods adopted from the semiconductor industry. Planar, high modulus substrates serve as supports for two dimensional device architectures that follow from high temperature growth/deposition processes and lithographic patterning. The resultant technologies are mechanically hard and brittle, with limited capabilities for biocompatible integration with the soft surfaces of the human body. Advances in fabrication techniques [17–21] and device designs [8,20,22–25], together with the recent emergence of high performance inorganic piezoelectric materials that have the mechanical attributes of plastics, create opportunities in piezoelectric devices with form factors and characteristics that are dramatically different from those previously attainable. Research over the last several years demonstrates possibilities in highly efficient and/or sensitive piezoelectric energy harvesters/sensors/actuators, with particular relevance in biomedical applications [20,26–32] and wearable electronics [33–37]. Furthermore, the discovery of high-performance, lead-free piezoelectric materials suggests bio/eco-compatible options that will further enhance opportunities [38–43].

This review highlights these advances, with an emphasis on underlying concepts in mechanics and associated engineering strategies in device construction. A short initial section summarizes the dual operating mechanisms of piezoelectrics. The content that follows highlights key design strategies for piezoelectric devices that adopt unusual mechanical attributes (flexible, stretchable) by virtue of optimized mechanical configurations (membrane strain engineering, wavy/buckled configurations), material chemistries (organics, inorganics and composites) and/or geometrical features (nanostructures, thin films). Component examples and system level demonstrators illustrate these ideas in mechanical energy harvesters, sensors and actuators. The collective results suggest a promising future for the combined use of piezoelectric materials and unusual mechanics concepts across a range of fields, particularly those in biomedical engineering.

2. Discussion

2.1. Coupled mechanical and electrical behaviors in flexible piezoelectric systems

The ability of piezoelectric materials to generate electrical power from mechanical deformations, and vice versa, originates from direct and indirect piezoelectric effects, respectively [1]. Bulk samples or thin films of piezoelectric materials typically serve as active components in rigid devices, for systems that exploit such effects in mechanical energy harvesting, sensing and actuation. The operating principles and design guidelines in flexible devices are different from those of conventional, rigid technologies. The essential mechanics concepts are most easily examined in device architectures that combine thin piezoelectric films on sheets of plastic. One recently reported example involves nanoscale ribbons (∼200 nm thicknesses) of PZT (lead zirconate titanate) created on a silicon wafer and then released by undercut etching of a sacrificial interfacial layer to allow integration onto thin flexible polyimide (PI) substrates with thicknesses of 75 μm by transfer printing [20]. In this type of system, the electromechanical behavior can be described via an analytical model in which compression by a distance ΔL at the ends leads to a curved shape (Fig. 1(a)) with an out of plane displacement given by $w = A[1 + \cos(2\pi x_1/L)]/2$, where A is the amplitude and L is the initial length of the device. The bending moment (M) is related to the curvature $\left(w''\right)$ as

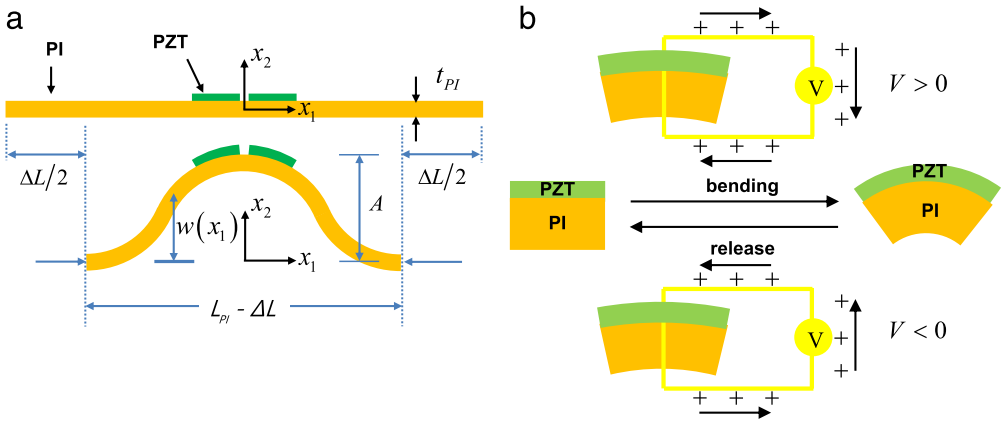

Fig. 1. Illustrations of coupling between the piezoelectric response of PZT nanoribbons mounted on a thin flexible substrate during bending, with definitions of variables used in theoretical analysis. Schematic illustration of (a) theoretical shape for the bending of such a system under compression and (b) charge movement during bending [44].

$M = \overline{EI}_{PI} w''$, where $\overline{EI}_{PI}$ is the plane-strain bending stiffness of substrate (PI). The curvature of the PZT nanoribbons can be written as $M/\overline{EI}_{comp}$, where $\overline{EI}_{comp}$ is the plane-strain bending stiffness of multi-layer device structure. When the lengths of the PZT nanoribbons are significantly smaller than that of the PI substrate, the curvature can be evaluated at $x_1 = 0$ (the center of PZT nanoribbons), and is given as $w'' = \left(-4\pi\sqrt{\Delta L/L}\right)/L$.

The in-plane strain determines the piezoelectric response, in particular the output voltage. The total strain is the sum of the membrane and bending strains, whereas the bending strain is tensile/compressive on the opposite sides with equal magnitude across the thickness and therefore does not contribute to the voltage. The membrane strain [44], which is the axial strain at the center of PZT nanoribbons, is

$$\varepsilon_m = 4\pi \frac{\overline{EI}_{PI}}{\overline{EI}_{comp}} w'' h, \tag{1}$$

where h denotes the distance from the midpoint of the thickness of the PZT layer to the neutral mechanical plane (NMP; plane of zero bending induced strain). The location of the NMP in such a multi-layer structure is $y_{neutral}$, given as [20]

$$y_{neutral} = \frac{\sum_{i=1}^{n} \bar{E}_i t_i \left(2\sum_{j=1}^{i} t_j - t_i\right)}{2\sum_{i=1}^{n} \bar{E}_i t_i}, \tag{2}$$

where $\bar{E}_i$ and t_i are the plane-strain modulus and thickness of the i^{th} layer ($i = 1$ represents the 1^{st} layer of the bottom structure). The value of h is important in the design of flexible piezoelectric systems for sensing and mechanical harvesting, where the goal is to maximize the electrical response and/or the degree of bendability while maintaining the strain below the fracture thresholds of the active materials.

In certain applications, the plane-strain bending stiffness is also important. The stiffness of the system considered here, with and without the PZT and associated electrodes, can be written

$$\overline{EI}_{PI} = \left(\bar{E}_{PI} h_{PI}^3\right)/12, \tag{3}$$

$$\overline{EI}_{comp} = \sum_{i=1}^{n} \bar{E}_i t_i \left[\frac{t_i^2}{3} + \left(\sum_{j=1}^{i} t_j - y_{neutral}\right) \times \left(\sum_{j=1}^{i} t_j - y_{neutral} - t_i\right)\right], \tag{4}$$

respectively, where $i = 1$ represents the first bottom layer in the structure, h_{PI} and $\bar{E}_{PI}$ are the thickness and plane-strain modulus of PI, respectively. Selecting appropriate values of h and the plane-strain bending stiffness parameters (i.e., engineering the membrane strain) offers a route to configure the device design for high system flexibility while generating optimal amounts of electrical power.

The direct piezoelectric behavior (i.e., piezoelectric voltage output due to buckling deformation) defines this power, and is governed by the equation that relates the stress (σ_{ij}), strain (ε_{ij}), electrical field (E_i), and electrical displacement (D_i). For a film of PZT with the polarization in the thickness direction (x_3), the plane-strain deformation ($\varepsilon_{22} = 0$) and the associated stress ($\sigma_{33} = 0$) from the traction free boundary condition on the top surface, the electrical displacement along x_3 is defined as $D_3 = \bar{e}\varepsilon_{11} + \bar{k}E_3$, where $\bar{e} = e_{31} - (c_{13}/c_{33})\, e_{33}$ and $\bar{k} = k_{33} + \left(e_{33}^2/c_{33}\right)$ are the effective piezoelectric constants, and e_{ij}, c_{ij} and k_{ij} are the piezoelectric, elastic and dielectric parameters of PZT, respectively [2]. An analytical model for coupling between the piezoelectricity and the buckling deformation defines the role of membrane strain and also the importance of internal resistance of the voltmeter used for measurement, as shown in Fig. 1(b). The electrical displacement of the system can be rewritten as $D_3 = \bar{e}\varepsilon_m + \frac{\bar{k}V}{Nh_{PZT}}$, where V is total voltage between the two ends of the N groups of PZT ribbons connected in series, h_{PZT} is the thickness, and ε_m is the membrane strain of the PZT ribbon. The current is $I = -A_{PZT}\dot{D}_3$, where A_{PZT} is the total area of the PZT ribbons in a group. With Ohm's Law,

$V/R = -A_{PZT}\dot{D}_3$, i.e.,

$$\frac{dV}{dt} + \frac{Nh_{PZT}}{A_{PZT}R\bar{k}}V = -\frac{N\bar{e}h_{PZT}}{\bar{k}}\frac{d\varepsilon_m}{dt}. \tag{5}$$

For a representative strain $\varepsilon_m = \left[1 - \cos\left(2\pi\bar{t}\right)\right]/2$, the dimensionless voltage is

$$\bar{V} = \frac{\pi\bar{R}}{\sqrt{1+4\pi^2\bar{R}^2}}\sin\left[2\pi\bar{t} - \arctan\left(2\pi\bar{R}\right)\right] + \frac{2\pi^2\bar{R}^2}{1+4\pi^2\bar{R}^2}e^{-\bar{t}/\bar{R}}, \tag{6}$$

where the first part of the equation is a periodic function that alternates between positive and negative, and the second part is an exponential decay [44]. This equation indicates clearly that the measured voltage output depends on the internal resistance of the voltmeter as well as the membrane strain. This point is often overlooked in literature reports of flexible piezoelectric devices.

For energy harvesting, the efficiency of conversion of mechanical to electrical energy is a vital parameter [7]. One approach defines the efficiency as

$$\eta = \frac{W_{stored}}{W_{strain}} \times 100\%, \tag{7}$$

where W_{stored} is the energy stored and W_{strain} is the total strain energy the piezoelectric material. A more realistic treatment considers all components of the overall system (i.e., both active materials and the supporting substrate) [20,45] as

$$\eta = \frac{W_{stored}}{W_{total}} \times 100\%, \tag{8}$$

where W_{total} is the total mechanical work during the device bending. Here, the mechanical work on the system includes the effects of the piezoelectric layer together with the associated electrodes and device substrate. In this formulation, the efficiency depends on not only the properties of the piezoelectric material, but also the other elements of the devices as well as the overall architecture [20].

As an example of the utility of the mechanics theory reviewed here, published reports on flexible PZT harvesters designed to capture electrical power from motions of the heart, diaphragm and lung [20] show that it is possible to optimize the device construction to simultaneously achieve (1) low bending stiffness (0.22 N·mm and 0.10 N·mm for areas with and away from the PZT structures) to avoid unwanted mechanical load on the body, (2) high degrees of bendability (2.5 cm of bending radius) to conform to the targeted regions of the anatomy and (3) efficiencies sufficiently high (~2%) to generate power for operating a pacemaker (several microWatts).

Related devices exploit both the direct and indirect piezoelectric mechanisms to yield flexible sensors and actuators capable of measuring the moduli of soft materials [2]. Here, a sinusoidal voltage applied to an actuator induces mechanical motions in the piezoelectric layer (i.e., indirect piezoelectric effect), the substrate materials and a contacting surface (i.e., the object under test). Neighboring sensors detect these motions, via the amplitude and the phase of their induced voltages (i.e., direct piezoelectric effect).

The indirect piezoelectric effect in an actuator under a constant voltage (U_A) induces an expansion, Δu, that can be determined by considering the plane-strain deformation ($\varepsilon_{22} = \varepsilon_{12} = \varepsilon_{23} = 0$), the electric field boundary condition ($E_1 = E_2 = 0$), and the traction free condition ($\sigma_{33} = 0$) according to

$$\Delta u = \beta_1 \frac{e_{33}}{c_{33}}U_A, \tag{9}$$

where β_1 is dimensionless parameter that depends on the materials properties and the geometries of the device layers.

The direct piezoelectric effect in adjacent sensors induces voltages with magnitudes and temporal behaviors determined by mechanical coupling to the actuator, through the device structure itself and the material under test. The output voltage of the i^{th} sensor can be written

$$U_{S,i} = \beta_2 \frac{p_{S,i} \cdot h_{PZT}}{e_{33}}, \tag{10}$$

where h_{PZT} is the thickness of PZT ribbon, β_2 is dimensionless parameter that depends on the material properties and geometries of the device layers, $p_{S,i}$ is the average stress induced by the actuator on each of the other elements in the array [2,46]. The relationship between the sensor voltage output and the applied actuation voltage can be obtained by rewriting of Eq. (10), to give

$$U_{S,i} = \alpha \frac{h_{PZT}}{2a}\frac{E_{P.S.}}{c_{33}}U_A, \tag{11}$$

where $\alpha = \beta_1 \cdot \beta_2 \cdot \eta_i$, $2a$ is the width of sensor, $E_{P.S.}$ is the storage (elastic) modulus of the substrate under test, and η_i is a dimensionless parameter. When other parameters are known or measured, Eq. (11) can be used to determine the modulus of a sample ($E_{P.S.}$) under test.

Considering the stratified structure of human skin, Yuan et al. [47] extended this method of measuring [2] the Young's modulus. Here, a similar device contains only one pair of piezoelectric actuator and sensor for simultaneously determining the Young's moduli of the epidermis and dermis layers as well as the epidermis thickness. The ratio of the output voltage U_{output} of the sensor and input voltage U_{input} applied on the actuator equals to a function of effective piezoelectric constants ($\bar{e}$, $\bar{k}$), geometry parameter of the sensor (b), and the moduli of encapsulation layer (E_{encap}) and epidermis layer ($E_{epidermis}$), as

$$\frac{U_{output}}{U_{input}} = -\frac{\pi^2}{6}\frac{\bar{e}^2 h_{PZT}/\bar{k}}{K_s}\frac{\left(E_{encap} + E_{epidermis}\right)b}{K_s}C_1^s, \tag{12}$$

where, the C_1^s is a dimensionless coefficient that depends on the Young's moduli of the epidermis and dermis and the thickness of epidermis [47]. The elastic and geometry properties of the layered structure of human skin can be determined by Eq. (12).

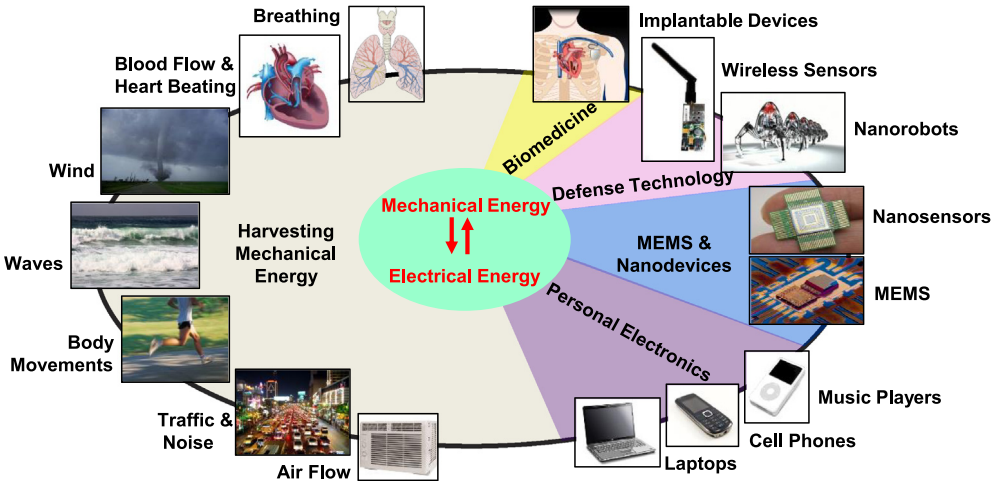

Fig. 2. Possible sources of energy for harvesting (left) and opportunities use of this energy in sensing and actuation (right) that can be considered for flexible/bendable piezoelectric devices.
Source: The figure is adapted from [49].

These and other modes of operation in unusual piezoelectric devices offer the basis for diverse applications in biomedicine, defense technology, nano-devices, microelectromechanical systems (MEMS), personal electronics and mechanical energy harvesters (MEHs) [48,49]. Fig. 2 summarizes a range of examples, achieved in some cases by using nanoscale inorganics and in others with emerging classes of organic piezoelectrics [49]. The following section highlights some examples of the material choices.

2.2. Inorganic piezoelectric materials

The devices used to introduce the key considerations outlined in the preceding section have, as a key feature, small thicknesses in both the active materials and the substrates. As previously noted, fabrication of PZT nanoribbons follows from lithographic patterning and lift-off of thin film material precursors cast and cured at high temperatures on rigid substrates, often silicon wafers. The lift-off process typically involves a buried sacrificial layer of silicon dioxide (SiO_2) or magnesium oxide (MgO) [19,20,50] such that chemical etching processes can initiate release for delivery to a target substrate by transfer printing [51]. Other approaches use high power laser exposures through transparent substrates such as sapphire [21], where absorption of nanosecond pulses of light induces transient heating and resulting interface failure between the piezoelectric layer and the substrate. As with chemical lift-off, transfer printing provides a means for manipulating the released films and integrating them into functional systems [52,53] with exceptional performance. Films of barium titanate ($BaTiO_3$), of interest for their high piezoelectric constant (d_{33} of 105 pm/V) [17,54], can also be manipulated using similar strategies.

Other synthetic methods to form piezoelectric materials with nanoscale thicknesses rely on evaporation, as in the case of zinc powder to yield zinc oxide nanowires (ZnO NWs) [55] or on solution phase synthesis methods based on microemulsion and hydrothermal growth, for the case of ZnO NWs [56], nanodiscs or nanorings [22]. In many examples, these strategies can be applied at low temperatures directly on substrates of interest or delivered to them via printing processes [7]. The morphologies and resulting properties of piezoelectric nanostructures depend on the synthesis conditions [22]. In some cases, such as those with ZnO, finite size effects enhance the effective piezoelectric constants compared to their bulk counterparts [57–59]. For instance, films of ZnO formed by sputter deposition (d_{33} = 14 pm/V) [45], and ZnO nanobelts (d_{33} = 14.3–26.7 pm/V) formed by growth have larger piezoelectric constants than those of bulk ZnO (d_{33} = 9.93 pm/V) [58]. Likewise, the hydrothermal method can yield $BaTiO_3$ nanotubes (diameter of 11.8 ± 2.3 nm, and length of 4.1 ± 1.2 μm) with grain sizes of ∼1 μm and piezoelectric constants (d_{33}) up to 460 pm/V [60,61], which is approximately four times higher than that of poled thin films of $BaTiO_3$ [17].

Another example of low temperature deposition is reactive sputtering, for use with piezoelectrics such as aluminum nitride (AlN) [62]. The resulting films tend to form with a high degree of (0001) orientation at room temperature, thereby enabling direct deposition and device fabrication on desired target substrates, such as polymers. Such AlN layers can exhibit piezoelectric constants (d_{33}) of 0.7 pm/V [62]. Other routes to piezoelectric materials, particularly nanowires/fibers, exploit electrostatically induced ejection of liquid precursors through fine nozzles, in an approach known as electrospinning. Here, the resulting materials exhibit enhanced piezoelectric properties associated with highly oriented dipole construction that follows from the spinning process, along with high flexibility and associated mechanical strength [63]. PZT nanofibers formed in this way exhibit a piezoelectric constant (d_{33}) of 83.4 pm/V, which is higher than that of PZT films with the same composition (d_{33} < 55 pm/V) [64].

In all cases, such materials can be incorporated onto compliant substrates by processes of transfer printing to form flexible and/or stretchable devices. Advanced embodiments involve forming the materials into wavy/buckled geometries (Fig. 3(c), (d)), bonded to elastomer substrates

such as polydimethylsiloxane (PDMS). The result is a structure that can be stretched to large levels of strain without fracture [19,65]. Here, the wavy/buckled formats allow the system to adapt to applied strain through changes in the structure geometries, while the substrate provides an elastic restoring force. In this configuration, the wavy PZT exhibits enhanced piezoelectric constant ($d_{33} = 130$ pm/V) compared to that in its flat geometry ($d_{33} = 75$ pm/V) [19]. In one example, thin ribbons of PZT bonded to a prestrained slab of PDMS [19] transform into wavy configurations upon release of the prestrain. The buckling parameters (e.g., wavelength (L) and amplitude (A) of sinusoid buckled region) can be estimated by determining the total energy in the system (i.e., the sum of energy from the uniaxial strain in the ribbon, as a result of bending, and the adhesion energy between piezoelectric material and polymer substrate). An analytical treatment [19] gives

$$L = \frac{\pi h_{PZT}}{\left[\frac{\varepsilon_{pre}}{1+\varepsilon_{pre}} - \sqrt{\left(\frac{\varepsilon_{pre}}{1+\varepsilon_{pre}}\right)^2 - \frac{6w_{ad}}{Eh_{PZT}}}\right]^{0.5}}, \tag{13}$$

$$A = \frac{2L_o}{\pi}\sqrt{\frac{\varepsilon_{pre}}{1+\varepsilon_{pre}} - \frac{\pi^2 h_{PZT}^2}{3L_o^2}}, \tag{14}$$

where h_{PZT} is the thickness of the PZT ribbon, w_{ad} is the adhesion energy (per unit area) between PZT and PDMS, E is the Young's modulus of PZT, ε_{pre} is the prestrain of PDMS, and L_o is the length of original flat ribbon.

Not only can this geometry enhance the mechanics, but it also provides a unique opportunity in actuation. Specifically, when implemented with a capacitor-type structure of Pt/Cr/PZT/Pt/Ti layers [65], the application of a voltage, V to the top and bottom electrodes induces a buckling at $V = V_{crit}$ and even further modulates the existing buckling displacement at $V \geq V_{crit}$, characterized by $u_3 = A\cos(2\pi x_1/\lambda)$ with

$$\lambda = 2\pi h_{PZT}\left[\frac{\bar{E}}{\bar{E}_s}\left(1 + \frac{\bar{e}^2}{\bar{E}\bar{k}}\right)\right]^{1/3}, \tag{15}$$

$$A = h\left(1 + \frac{\bar{e}^2}{\bar{E}\bar{k}}\right)^{1/2}\sqrt{\frac{V}{V_{crit}-1}} \quad \text{for } V \geq V_{crit}, \tag{16}$$

where $\bar{e}$ and $\bar{k}$ are the effective piezoelectric constants, h_{PZT} is the thickness of PZT (piezoelectric) ribbon, $\bar{E}$ is the plane-strain modulus, $\bar{E}_S$ is the strain modulus of PDMS, V is the electrical potential voltage, and V_{crit} is the critical voltage for the thin film to buckle. The amplitude of displacement realized in this fashion can significantly exceed that possible for an otherwise similar PZT stack on a rigid substrate, obtained from $(e_{33}/c_{33})V$, where e_{33} and c_{33} are piezoelectric and elastic constants, respectively.

Even in flat non-buckled geometries, the piezo response on deformable substrates can exhibit enhancements. As an example, piezoelectric (PZT) devices built on PDMS exhibit more than two orders of magnitude greater voltage output than otherwise identical devices on silicon [50]. The improvement arises from differences in mechanics. In particular, deformation of PZT on Si mainly involves simple, uniaxial compression along the thickness direction. By comparison, PZT on PDMS includes complex and three-dimensional deformations. The relationship between the deformation and the voltage can be defined as

$$V_{PZT} = \alpha A_{contact} P, \tag{17}$$

where P is the applied pressure, $A_{contact}$ is the contact area between the PZT and an applied weight, and α is a parameter that depends on the material constants for PZT and the deformation mechanics of the substrate. The value of α for PZT on Si is $\alpha = e_{33}h_{PZT}/\left[A\left(k_{33}c_{33} + e_{33}^2\right)\right]$, where h_{PZT} is the thickness of PZT ribbon, A is the total area of PZT, e_{33} is piezoelectric constant, c_{33} is elastic constant, and k_{33} is the dielectric constant. Here, α is 5.77×10^{-4} V/N. By comparison, the α for PZT on PDMS obtained through analysis with the Finite Element Method (FEM) is 0.068 V/N [50]. In this manner, soft substrates enhance not only the mechanics but also the voltage response in piezoelectric systems [66,67].

2.3. Organic and composite piezoelectric materials

Other routes to flexible and/or stretchable devices rely on unusual piezoelectric materials, rather than unusual geometries. In particular, recent developments allow high performance devices to be constructed from flexible organic and composite piezoelectric materials [3,5,6,8–10]. Fig. 4(a)–(h) show scanning electron microscope (SEM) images of examples in nanostructured, thin film, and textile formats. A popular example in flexible organic piezoelectrics is polyvinylidene fluoride (PVDF) and its copolymer, poly(vinylidene fluoride–trifluoroethylene) (PVDF–TrFE), particularly when processed into aligned fibers by electrospinning as shown in Fig. 4(a) or cast in anodic porous alumina (APA) templates as in Fig. 4(b). The fibers can be efficiently crystallized in the β-phase whose parallel alignment of dipoles leads to surface charge separation for enhanced piezo response [68]. These fibers have piezoelectric constants ($d_{33} \sim -57.6$ pm/V) that are typically higher than those of corresponding thin films ($d_{33} \sim 15$ pm/V). In device examples, these materials can yield sensors with the capacity to measure pressures as low as 0.1 Pa, for applications in robotics, high sensitivity touch interfaces [3] and nanoscale actuators [6].

Thin films of PVDF–TrFE are nevertheless valuable due to the ease with which they can be spin cast over large areas with minimal surface roughness and excellent uniformity, as shown in Fig. 4(c). In this format, the high level of β-phase content leads to strong piezoelectric behavior. In one study, thin films of PVDF–TrFE (1 μm) exhibit higher β-phase content than thick films (6 μm) under untreated conditions (without any mechanical stretching or electrical poling) [9]. Thin films experience increased surface tension during spin coating, which results in improved crystallinity. In device examples, the PVDF–TrFE thin films can serve as active elements in pressure sensors with fast recovery times (0.17 ms) and an operating pressure range of 0–30 mmHg, suggesting potential applications in flow sensing for implantable biomedical applications [9].

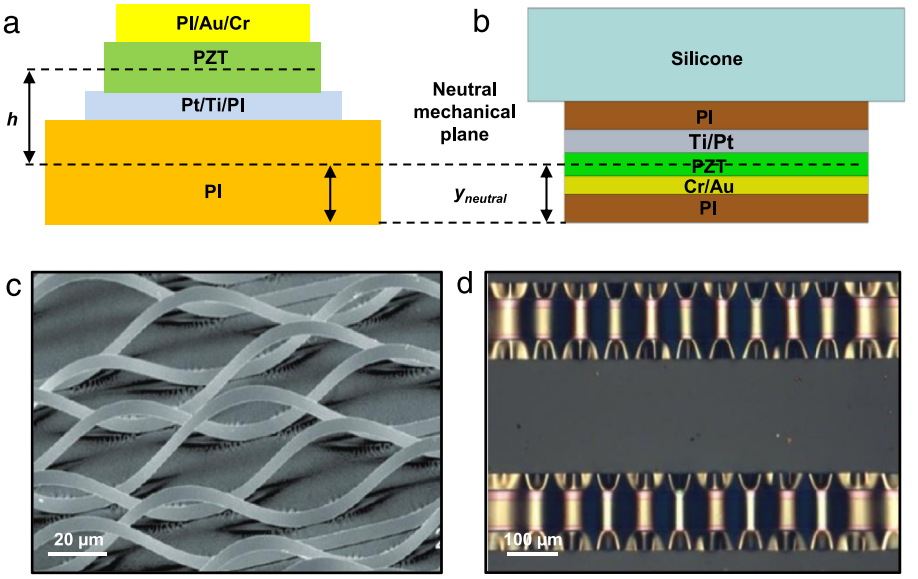

Fig. 3. Mechanics of flexible/stretchable piezoelectric devices. Illustrations of the location of the neutral mechanical plane relative to the piezoelectric materials for (a) a flexible MEH [20] and (b) a stretchable sensor [2]. (c) SEM image of wavy PZT nanoribbons on a PDMS substrate [19]. (d) Optical microscope image of wavy PZT nanoribbons with electrodes on a PDMS [65].

Piezoelectric fibers can even be integrated into woven textiles to yield an attractive platform for wearable applications. For instance, PVDF monofilaments serve as spacers that connect the top and bottom electrodes of silver coated polyamide 66 (PA 66) multifilament yarns as shown in Fig. 4(d). For this example, a high content (∼80%) of β-phase results from melt spinning and fiber drawing. Integration of these PVDF monofilaments with electrodes via a knitting technique yields a textile based piezoelectric that has comparable flexibility to conventional fabrics [69]. Other types of platforms rely on gold coated textile substrates of polyester as top and bottom electrodes integrated with ZnO NWs and polyethylene (PE). In this platform, electrostatic energy is generated from the interaction between the PE film and gold coated textile. Energy from the piezoelectric effect results from mechanical deformation of the ZnO NWs. The coupling between these two mechanisms provides a hybrid system (Fig. 4(h)) that improves overall system performance, particularly the output voltage, for wearable applications [70].

Inorganic/organic composites are also of interest, owing to the ability to adjust the ratio of the component materials to achieve desired properties. For example, incorporating high performance PZT fibers (d_{33} = 127 pm/V) [71] into a polymer matrix produces a composite with a good balance between electrical performance and mechanical properties. Electrospinning of an aged sol–gel PZT solution and polyvinyl-pyrrolidone (PVP) yields fibers with controlled diameters. The PVP defines the viscosity, such that increasing the concentration of PVP increases the diameter of the fibers. Nanofibers formed from PZT/22 weight% PVP solution (Fig. 4(e)) have diameters of ∼300 nm [5]. The fiber diameter associated with ceramic/polymer weight ratio can be engineered to obtain the desired mechanical flexibility in addition to optimum piezo response.

Inorganic piezoelectric nanostructures based on other materials such as PMN-PT ((1-x) $Pb(Mg_{1/3}Nb_{2/3})O_3$-$xPbTiO_3$) can also be formulated into polymer matrices to take advantage of features of both piezoelectric nanostructures and polymers. PMN-PT NWs have a piezoelectric constant (d_{33} = 371 pm/V) that is approximately three times higher than that of PZT fibers [72]. The formation of PMN-PT NWs via hydrothermal synthesis can yield a three-dimensional branched structure, as shown in Fig. 4(f). Integration of such structures into a matrix of PDMS allows an efficient transfer of stress from the polymer to the NWs (along the polarized direction of piezoelectrics) that enhances the output power performance. Our finite element analysis (FEA) confirms this conclusion for a hierarchical (branch) structure consisting of three nanowires embedded in a polymeric (PDMS) matrix, each with the dimension 10 μm (L) × 0.5 μm (W) × 0.5 μm (T). Each nanowire is oriented 120° with respect to the other two, and all are 45° to the electrode surface. The matrix is 100 μm (L) × 50 μm (W) × 15 μm (T) and is coated with a (0.2 μm thickness) polyimide (PI) encapsulation layer on the top and bottom surfaces, where the compression is applied. The results show that the hierarchical (branch) structure increases the strain (along the polarized direction of piezoelectrics) transferred to the nanowires by 30% (than the design of three separated NWs with same geometry and orientations). The efficiency of mechanical impact transfer is particularly enhanced when the hierarchical structure PMN-PT NWs is perpendicularly aligned between top and bottom electrodes. This structure, therefore, offers promising applications especially in energy harvesters and sensors.

Alternative types of composites use inorganic piezoelectric particles, formed in one case by surface modifications and a sequential layer formation to achieve up to 95 weight% loading of PZT particles in thin films of epoxy based polymers (Fig. 4(g)). Surface modification of the PZT involves isophorone diisocyanate and polyoxyalkyleneamine, to yield molecular entanglement with the epoxy molecules and covalent bonding to the epoxide groups. The

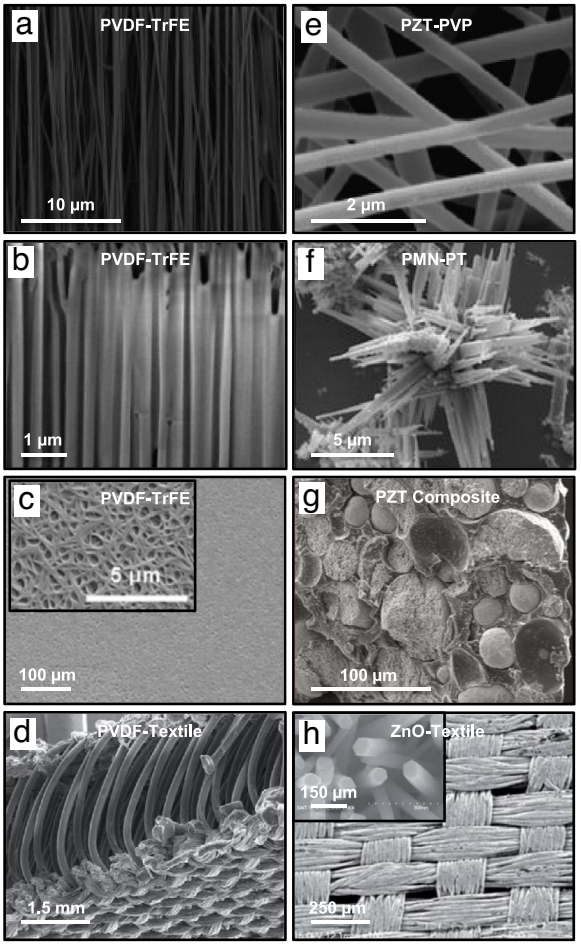

Fig. 4. SEM images of organic materials and composite systems with various structures. Image of (a) PVDF–TrFE fiber array generated from electrospinning [3], (b) PVDF–TrFE nanowires cast in APA template [6], (c) PVDF–TrFE thin film with a magnified view in the top inset [9], (d) woven PVDF fibers with conductive yarns as a piezoelectric fabric [69], (e) PZT–PVP fibers with 22 weight% PVP [5], (f) hierarchical structure of a PMN-PT nanowire bundle [72], (g) PZT/epoxy composite in thin film format [10], and (h) grown ZnO nanowires on textile fabric with an inset of grown ZnO NWs [70].

result enables uniform dispersion and with strong particle/matrix interfaces. The resultant PZT composite offers advantages, such as shorter poling time, lower poling voltage (up to 75%), and higher piezoelectric constant (d_{33} = 12 pm/V) than the corresponding unmodified piezocomposite [10].

2.4. Inorganic piezoelectric devices in biomedicine

Among the many applications for piezoelectric technologies, those that involve interfaces with the human body represent an area of rapid development. Inorganic piezoelectric materials, appropriately configured into flexible/stretchable formats using concepts outlined in the previous sections, are preferred due to their high piezoelectric coefficients. For example, recent work demonstrates a range of different types of devices capable of harnessing electrical energy from mechanical energy resources, each with potential applications in biomedicine, as in Fig. 5.

Some of the most intensively studied classes of bio-integrated, flexible mechanical energy harvesters involve ZnO. Images associated with a device that incorporates horizontally aligned ZnO NWs appears in Fig. 5(a). As described in the Section 2.2, nanoscale effect on ZnO NWs enhances the effective piezoelectric constant compared to that of bulk forms and provides flexibility to the MEH structure. Under alternating bending/unbending motions with peak strains of 0.1% and strain rates of 5% s^{-1}, devices with active areas of 1 cm^2 generate peak voltages of ∼2.0 V (Fig. 5(b)) and currents of ∼100 nA, sufficient to operate a commercial LED [7]. ZnO is particularly unique because it dissolves in biofluids, with biocompatible end products. As a result, the devices based on ZnO film built with other bioresorbable materials such as magnesium for the electrodes and interconnects, and silk fibroin for the substrates yield completely bioresorbable devices (Fig. 5(c)). Examples include devices with areas of 1 × 2.5 cm^2 that are capable of generating voltages and currents of 1.14 V (Fig. 5(d)) and 0.55 nA, respectively, under a peak strain of 0.056% [45]. Envisioned uses are in biodegradable electronic implants for internal wound care, pain management, temporary cardiac pacing and others.

By comparison to ZnO, perovskite piezoelectric materials such as $BaTiO_3$ are appealing due to their higher piezoelectric constants [17,54]. As discussed in Section 2.2, the use of soft lithography and transfer printing techniques facilitate the integration of $BaTiO_3$ MEHs into thin film formats on substrates of interest, as shown in Fig. 5(e) [17]. In this configuration, the MEHs (areas of 1 cm^2) are flexible while maintaining their high piezoelectric properties and are capable of generating peak output voltages and currents of 0.4 V (Fig. 5(f)) and 12 nA, respectively, under peak strains of 0.55% and strain rates of 1.6% s^{-1}. Another example involves the incorporation of $BaTiO_3$ NWs synthesized via hydrothermal methods into PDMS (Fig. 5(g)). Here, increasing the NW composition (greater than 20 weight%) degrades the electromechanical coupling and leads to low output voltages [73]. With an optimum amount (20 weight%) of NWs and an area of 3 × 4 cm^2, this type of MEH can achieve peak output voltages of 7.0 V (Fig. 5(h)) and currents of 360 nA under peak strains of 0.33%.

PZT is another perovskite material, of interest due to its high piezoelectric constant. As described previously, flexible devices that use arrays of PZT nanoribbons in optimized architectures for deployment on large-scale animal models (e.g. cow, sheep, and pig) provide sources of electrical power for implants such as cardiac pacemakers. MEHs with areas of 2 × 2.5 cm^2 mounted onto epicardial sites of the beating heart of a bovine (cow) model are shown in Fig. 5(i). Here, the value of h and the plane-strain bending stiffness parameters are arranged in such a way to achieve high system flexibility while producing optimal amounts of electrical power (see the Section 2.1). For instance, under peak strains of 0.35%, output voltages can reach ∼3.7 V. Different power outputs are also observed as a result of affixing the MEH onto different locations of heart, such as the free wall, right and left ventricles, consistent with the anatomy and the

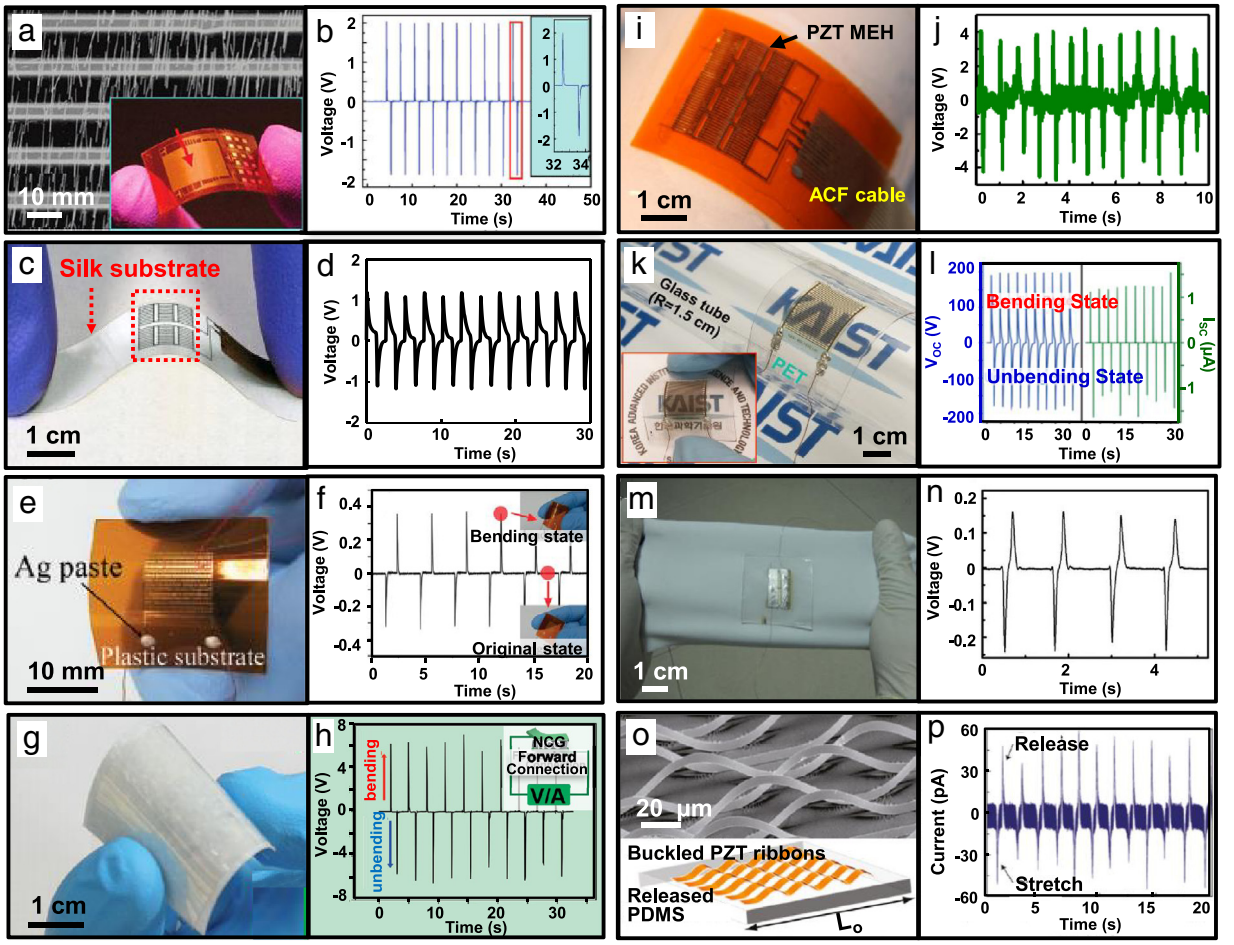

Fig. 5. Flexible and stretchable MEHs with various piezoelectric materials. (a) SEM image of horizontally aligned ZnO NWs on a plastic substrate with an inset of the resultant device [7]. (b) Output voltage from a ZnO NW MEH during bending/unbending [7]. (c) Photograph of a biocompatible ZnO MEH under compression [45]. (d) Output voltage from a ZnO MEH during bending/unbending [45]. (e) MEH based on a thin film of $BaTiO_3$ [17]. (f) Output voltage from a $BaTiO_3$ MEH during bending/unbending [17]. (g) MEH based on nanowires of $BaTiO_3$ [73]. (h) Output voltage from a $BaTiO_3$ nanowire MEH during bending/unbending [73]. (i) MEH based on nanoribbons of PZT [20]. (j) Output voltage from a PZT nanowire MEHs during motions while mounted on a bovine right ventricle [20]. (k) MEH based on a large-area, thin film of PZT released by LLO, an inset showing the resultant device manually bent [21]. (l) Output voltage from a LLO transferred thin-film PZT MEH during bending/unbending [21]. (m) MEH formed using textile-based PZT [34]. (n) Output voltage from a textile-based PZT MEH under the stretching and releasing motions [34]. (o) SEM image (top) and schematic diagram (bottom) of a stretchable MEH based on wavy PZT nanoribbons [19]. (p) Output current of a stretchable, PZT based MEH under stretching motions [19].

nature of motions associated with beating. The open circuit voltage for the case of the right ventricle reaches ~4 V (Fig. 5(j)) [20]. A mechanically stacked collection of five such MEHs yields an average power density of 1.2 $\mu W/cm^2$, which is sufficient to operate a cardiac pacemaker. A key design consideration is that these MEHs have minimal bending stiffnesses, as discussed in the Section 2.1, to minimize mechanical loads on the heart, thereby avoiding arrhythmic behaviors associated with device-induced physical constraints. Similar devices can harness mechanical energy from the natural motions of other organs, such as lung and diaphragm [20]. Other similar *in vivo* experiments have also been demonstrated to capture the mechanical energy from diaphragm and heart of small animals (i.e., rats) with ZnO NW [26] and PMN-PT based MEHs [28].

Further improvements in performance are possible via the use of uniform, large-area films of PZT (Fig. 5(k)) released by laser lift-off (LLO) [21]. The LLO process minimizes the structural damage on the PZT thin film, as a result of immediate recrystallization after vaporization by laser irradiation. This device in Fig. 5 demonstrates the capability of the LLO process, which allows large area PZT device fabrication without any electrical and mechanical degradation in the piezoelectric film (see the Section 2.2). With device areas of 1.5×1.5 cm^2, the output voltages can reach ~200 V under bending deformations (peak strain of 0.386% and strain rate of 2.32% s^{-1}), as shown in Fig. 5(l). Slight human finger motions, in fact, can light as many as 100 blue LEDs simultaneously.

Compared to flexible platforms, stretchable mechanics can increase the breadth of options for applications, particularly in wearable devices that cover large areas of internal organs. One stretchable example employs a textile composed of PZT fibers formed by electrospinning in Fig. 5(m) [34]. By virtue of the electrospinning process

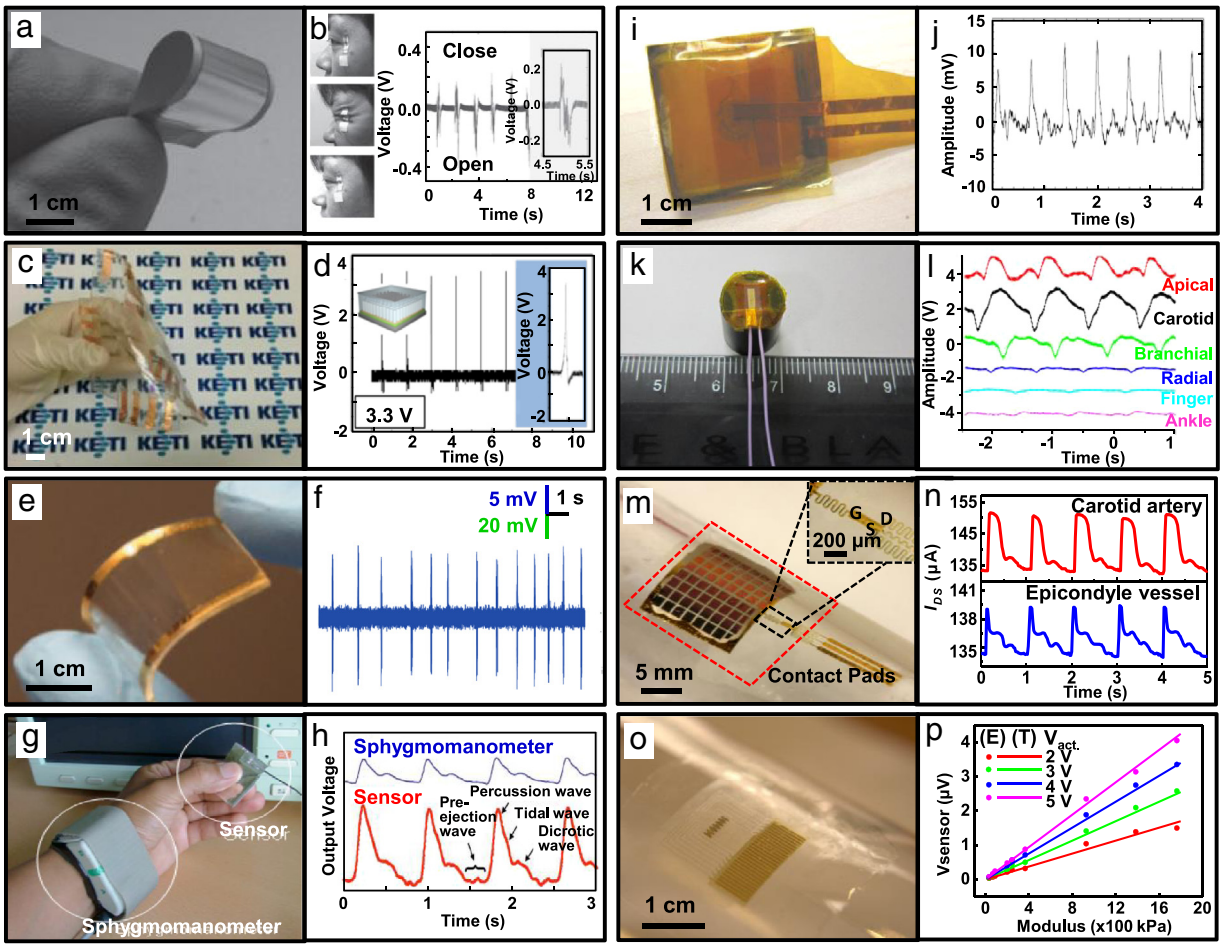

Fig. 6. Various piezoelectric sensors and actuators in flexible and stretchable formats. (a) A flexible active sensor made of ZnO NW arrays grown on ultrathin aluminum foil [74]. Output voltage from this device, driven by the blinking of the eye [74]. (c) Touch sensor based on ZnO NWs and $BaTiO_3$ capping layers [54]. (d) Voltage response of the touch sensor [54]. (e) A flexible PZT nanoribbon designed to monitor cellular deformations [76]. (f) The corresponding voltage response of PZT nanoribbons under cellular deformation [76]. (g) AlN pressure sensor and sphygmomanometer to measure blood pressure pulse waves from the wrist [62]. (h) Pulse waveform signals generated using this AlN pressure sensor and sphygmomanometer [62]. (i) Piezoelectric membrane sensor based on PZT [77]. (j) Voltage response of the sensor attached to the wrist, measuring pressure pulse waves [77]. (k) Flexible piezoelectric tactile sensor [78]. (l) Diverse pulse amplitude and waveforms detected by this flexible tactile sensor at various regions of the human body [78]. (m) Photograph of a PZT pressure sensor wrapped on a cylindrical glass support with an inset image of stretchable conducting traces [50]. (n) Current responses measured from the carotid artery and epicondyle vessel [50]. (o) Array of stretchable PZT actuators and sensors on a polymer substrate wrapped on a cylindrical glass support [2]. (p) Output voltage as a function of the substrate modulus recorded at four actuation voltages [2].

described in the Section 2.2, PZT fibers have enhanced piezoelectric properties and high flexibility. In a device example with an area of 1.5×0.8 mm^2 stretching/releasing motions create output voltages of ∼0.24 V (Fig. 5(n)) and currents of 2.5 nA. An enhanced output can be achieved by optimizing the thickness and the hardness of the PDMS, which is the interface layer that bonds the PZT textiles and the fabrics. A different stretchable platform based on PZT involves transfer printing of PZT nanoribbons-onto pre-strained PDMS substrates to create wavy structures as in Fig. 5(o) [19]. Periodic stretching/releasing motions to peak strains of 8% yield currents of ∼50 pA from a system that consists of ten PZT nanoribbons (Fig. 5(p)). Here, the wavy structures not only enhance the piezoelectric constant as discussed in Section 2.2, but they also can accommodate tensile strains that are several orders of magnitude larger than those that induce fracture in otherwise similar ribbons in flat geometries. Such systems provide promising platforms for wearable energy harvesting where reversible stretchability is essential to operation.

Piezoelectric sensors and actuators integrated on soft tissues represent additional classes of systems of growing interest. The flexibility and/or stretchability of these devices afford new measurement capabilities on various curvilinear and soft surfaces. Fig. 6(a)–(p) show recent examples of piezoelectric sensors and actuators design for the skin and other tissues. In sensing modes based on the direct piezoelectric effect, such devices can detect and measure various physical deformations, ranging from those associated with touch to those induced by pulsatile blood flow. Lee et al. [74] reported a flexible sensor built using arrays of ZnO NWs on ultrathin aluminum foil substrate (18 μm; Fig. 6(a)) to detect human eye blinking. Although the skin deformations are small, sensors (5 ×

13 mm^2) generate easily measurable voltages of 0.2 V and currents of 2 nA as seen in Fig. 6(b). Piezoelectric materials can also be used in touch sensors, as demonstrated by devices based on ZnO NWs and a capping layer of $BaTiO_3$ (Fig. 6(c)). In this example, a single touch point-cell has an active area of 1×1 cm^2. The combination of these materials balances the high flexibility, modest piezoelectric constant in the ZnO NWs [75] with the comparatively brittle, high piezoelectric performance of the $BaTiO_3$ [54]. As shown in Fig. 6(d), the addition of $BaTiO_3$ capping layer enhances the sensitivity by increasing the signal response from 50 mV to ∼3.3 V under a normal force of 17 N applied via a linear motor. In this configuration, the sensor can also differentiate forces applied by a human finger, as a flexible touch sensor. Even the small deflections of single cells can be detected, where PZT nanomaterials can capture nanoscale deflections (∼1 nm) induced by forces imparted at the cellular scale [76]. Fig. 6(e) shows PZT nanoribbons printed onto a silicone substrate (an area of ∼1 × 2.5 cm^2) via transfer printing. Here, a standard whole-cell patch-clamp method induced mechanical deformations in individual PC12 cells. The voltage response (∼10 mV) of a PZT sensor shown in Fig. 6(f) demonstrates the device capability in detecting cellular deformations (∼1 nm).

Additional sensing modalities involve measurements of pressure pulse waveforms due to blood flow. Examples with the sensors composed of AlN film, formed via low temperature reactive sputtering, as described in Section 2.2, offer ability to detect pressures of ∼0.9 kPa, well within the sensitivity of the human finger to sense texture and shape (10–40 kPa). AlN is well suited for this application because it has high thermal and chemical stabilities [62]. A recent study compared AlN to a commercial sphygmomanometer as shown in Fig. 6(g). The pulse waveforms generated from the sensor at the fingertips, between the thumb and middle finger, are comparable to those collected at the wrist using a sphygmomanometer at a stress level of 10 kPa (Fig. 6(h)). This sensor can also detect tidal and pre-ejection waves that are critical for monitoring health and wellness. Another example uses stainless steel (SS) foil with thickness of 38 μm as the bottom electrode and substrate, with a layer of PZT (thickness of 70 μm) [77] encapsulated with polyimide (Fig. 6(i)). The PZT film, which exhibits a piezoelectric constant (d_{33}) of 37 pm/V at 10 kHz, allows detection of the mechanical displacements of the skin due to blood flow to generate pulse wave signals as shown in Fig. 6(j). In a similar example, PZT deposited onto a SS substrate by sol–gel processes with high temperature sintering (650 °C) and poling at high electric field (∼0.71 MV/m) yields a sensor with useful levels of performance (Fig. 6(k)) [78]. Mounting this type of PZT sensor on a plastic element allows sensing of bio-motions of various regions of the human body, such as carotid, brachial, radical artery, finger, and ankle artery. Fig. 6(l) shows the associated pressure waveforms. The collective results suggest a way to characterize the pulse wave velocity (PWV) as well as to diagnose hypertension and cardiac failure. The use of correct sets of materials, the engineering of device layouts, the integration of required electrical components and associated serpentine conducting traces allow construction of stretchable sensors. An example is shown in Fig. 6(m). This device consists of PZT nanoribbons with a total area of ∼22 mm^2 and serpentine connections provides system stretchability up to 30%. Dagdeviren et al. [50] studied the fundamental properties of this type of sensor, which has fast response time (∼0.1 ms) and high sensitivity (∼0.005 Pa), and applied it in various ways on human subjects. In this configuration, the NMP was engineered to be closer to the middle of PZT nanoribbons to minimize the bending induced in-plane strain (see the Section 2.1). As a result, the sensor can measure pressure accurately on any body parts that have curvatures larger than a few millimeters. In this study [50], the device captured changes in arterial pressure on a healthy female wrist. As previously discussed in the Section 2.2, the use of soft substrates enhances the mechanics due to complex and three-dimensional deformations, and result approximately in a hundred fold enhancement in the sensitivity. This high sensitivity allows use in determining PWV for arterial stiffness measurement by placing the sensors at two different locations of human body. Fig. 6(n) presents some relevant data on two different sites, such as the carotid artery and epicondyle vessel, with 2-min intervals and on three different human bodies. The resulting PWV of ∼5.4 ms^{-1} is similar to that measured using conventional tonometry.

In addition to sensing, mechanical actuation can be an important feature in biomedical devices. An example of a unique device platform includes ultrathin architectures of piezoelectric sensors and actuators, exploiting both direct and indirect piezoelectric mechanisms (see Section 2.1), combined with serpentine configurations of metal traces for electrical connections to measure the mechanical properties (e.g. elastic modulus) of soft tissues and organ systems [2]. Fig. 6(o) shows seven actuators (lateral dimensions of 200 × 1000 μm^2) and six sensors (lateral dimensions of 100 × 500 μm^2) that are made of PZT nanoribbons in capacitor type geometries sandwiched between two layers of electrodes. Here, bending onto curvy body parts has little effect on device operation since the NMP lies close to the middle of PZT nanoribbon, as discussed in Section 2.1. In this conformal modulus sensor (CMS) system, applying a sinusoidal voltage to an actuator mounted on the skin induces mechanical motions in the device structures and the underlying skin, which can then be detected by adjacent sensors. The voltage responses of these sensors provide information about the electromechanical coupling between the actuators and sensors, presenting ways to determine the mechanical modulus of the near surface region of the skin. The relationships between the sensor voltage output and modulus at 1 kHz can be seen in Fig. 6(p). The results show consistent linear proportionality between the modulus values of the substrates, for values between 30 and 1800 kPa, and associated sensor output voltages under various actuation voltages. The modulus can be determined from the actuator voltage, the sensor output voltage, the material properties and geometries of the device layers (see Section 2.1). In addition to *in vitro* and theoretical results, *in vivo* application of CMS on 30 patient volunteers demonstrate the system capabilities to detect changes in the elastic modulus of skin across the body due to dermatologic malignancies, which generally are stiffer than healthy tissues. The same system can also be used to measure the

modulus values of various biological tissues, such as the heart and the lung. As existing methodologies (e.g. torsion, traction and nanoindentation) to measure the mechanical properties of soft biological tissues are invasive and lack of microscale spatial resolution [2], the dual features to actuate and sense in a thin, conformal platform offer promising capabilities for fast, accurate, non-invasive diagnostics based on stiffness (i.e., human skin or other organs).

3. Conclusion and outlook

This review summarizes recent progress in piezoelectric technologies that rely on mechanics and materials concepts for functions that lie beyond those accessible with traditional approaches. Of the many enabled applications, those in biomedicine, for both clinical and research domains, appear particularly attractive. These advances follow directly from the dual operational mechanisms in piezoelectrics together with unusual mechanics strategies in device design, to allow physical properties that are compatible with intimately integration with the soft tissues of body. Other opportunities are in smart robotics and metrology tools. Parallel arrays of soft micromanipulators can be used to assemble micro- and nano-scale functional devices on a broad range of target substrates [79]. Related piezoelectric micro-robotic tools can perform complex tasks with nanometer precision [80], with potential in microbiology, micromachining and materials assembly. Piezoelectric micro-actuation provides a vacuum compatible, compact means for indentation, with high resolution for testing of fracture and plastic deformation in materials, even under electron microscope observation [81]. Collectively, the advancement in piezoelectric materials, fabrication techniques and device design mechanics will continue to afford new opportunities in wide ranging areas.

References

[1] I.R. Henderson, Piezoelectric Ceramics: Principles and Applications, APC International, Pennsylvania, USA, 2002.
[2] C. Dagdeviren, Y. Shi, P. Joe, R. Ghaffari, G. Balooch, K. Usgaonkar, O. Gur, P.L. Tran, J. Crosby, M. Meyer, Y. Su, R. Webb, A. Tedesco, M. Slepian, Y. Huang, J.A. Rogers, Conformal piezoelectric systems for clinical and experimental characterization of soft tissue biomechanics, Nature Mater. 14 (7) (2015) 1–11.
[3] L. Persano, C. Dagdeviren, Y. Su, Y. Zhang, S. Girardo, D. Pisignano, Y. Huang, J.A. Rogers, High performance piezoelectric devices based on aligned arrays of nanofibers of poly(vinylidenefluoride-co-trifluoroethylene), Nature Commun. 4 (1633) (2013) 1–10.
[4] X. Chen, S. Xu, N. Yao, Y. Shi, 1.6 V Nanogenerator for mechanical energy harvesting using PZT nanofibers, Nano Lett. 10 (6) (2010) 2133–2137.
[5] E.M. Alkoy, C. Dagdeviren, M. Papila, Processing conditions and ageing effect on the morphology of PZT electrospun nanofibers, and dielectric properties of the resulting 3–3 PZT/ polymer composite, J. Am. Ceram. Soc. 92 (11) (2009) 2566–2570.
[6] V. Cauda, S. Stassi, K. Bejtka, G. Canavese, Nanoconfinement: An effective way to enhance PVDF piezoelectric properties, ACS Appl. Mater. Interfaces 5 (13) (2013) 6430–6437.
[7] G. Zhu, R. Yang, S. Wang, Z.L. Wang, Flexible high-output nanogenerator based on lateral ZnO nanowire array, Nano Lett. 10 (8) (2010) 3151–3155.
[8] K.-I. Park, M. Lee, Y. Liu, S. Moon, G.-T. Hwang, G. Zhu, J.E. Kim, S.O. Kim, D.K. Kim, Z.L. Wang, K.J. Lee, Flexible nanocomposite generator made of $BaTiO_3$ nanoparticles and graphitic carbons, Adv. Mater. 24 (22) (2012) 2999–3004.
[9] T. Sharma, S.-S. Je, B. Gill, J.X.J. Zhang, Patterning piezoelectric thin film PVDF-TrFE based pressure sensor for cathether application, Sensors Actuators A 177 (2012) 87–92.
[10] N. Saber, Q. Meng, H.-Y. Hsu, S.-H. Lee, H.-C. Kuan, D. Marney, N. Kawashima, J. Ma, Smart thin-film piezoelectric composite sensors based on high lead zirconate titanate content, Struct. Health Monit. 14 (3) (2014) 214–227.
[11] L. Persano, C. Dagdeviren, C. Maruccio, L.D. Lorenzis, D. Pisignano, Cooperativity in the enhanced piezoelectric response of polymer nanowires, Adv. Mater. 26 (45) (2014) 7574–7580.
[12] C. Dagdeviren, M. Papila, Dielectric behavior characterization of fibrous-ZnO/PVDF Nanocomposite, Polym. Compos. 31 (6) (2010) 1003–1010.
[13] S.P. Beeby, M.J. Tudor, N.M. White, Energy harvesting vibration sources for microsystems applications, Meas. Sci. Technol. 17 (2006) R175–R195.
[14] S. Priya, D.J. Inman, Energy Harvesting Technologies, Springer Science, New York, USA, 2009.
[15] Z.L. Wang, Nanogenerator for Self-Powered Devices and Systems, Georgia Institute of Technology, Atlanta, USA, 2011.
[16] S. Terry, J.S. Eckerle, R.S. Kornbluh, T. Low, C.M. Ablow, Silicon pressure transducer arrays for blood-pressure measurement, Sensors Actuators A21–A23 (1990) 1070–1079.
[17] K.I. Park, S. Xu, Y. Liu, G.T. Hwang, S.J. Kang, Z.L. Wang, K.J. Lee, Piezoelectric $BaTiO_3$ thin film nanogenerator on plastic substrates, Nano Lett. 10 (12) (2010) 4939–4943.
[18] Y. Qi, N.T. Jafferis, K. Lyons, C.M. Lee, H. Ahmad, M.C. McAlpine, Piezoelectric ribbons printed onto rubber for flexible energy conversion, Nano Lett. 10 (2) (2010) 524–528.
[19] Y. Qi, J. Kim, T.D. Nguyen, B. Lisko, P.K. Purohit, M.C. McAlpine, Enhanced piezoelectricity and stretchability in energy harvesting devices fabricated from buckled PZT ribbons, Nano Lett. 11 (3) (2011) 1331–1336.
[20] C. Dagdeviren, B. Yang, Y. Su, P.L. Tran, P. Joe, E. Anderson, J. Xi, V. Doraiswamy, B. Dehdashti, X. Feng, B. Lu, R. Poston, Z. Khalpey, R. Gahffari, Y. Huang, M. Slepian, J.A. Rogers, Conformal piezoelectric energy harvesting and storage from motions of the heart, Proc. Natl. Acad. Sci. 111 (5) (2014) 1927–1932.
[21] K.-I. Park, J.H. Son, G.-T. Hwang, C.K. Jeong, J. Ryu, M. Koo, I. Choi, S.H. Lee, M. Byun, Z.L. Wang, K.J. Lee, Highly-efficient, flexible piezoelectric PZT thin film nanogenerator on plastic substrates, Adv. Mater. 26 (16) (2014) 2514–2520.
[22] F. Li, Y. Ding, P. Gao, X. Xin, Z.L. Wang, Single-crystal hexagonal disks and rings of ZnO: low-temperature, large-scale synthesis and growth mechanism, Angew. Chem. 116 (2004) 5350–5354.
[23] Z.L. Wang, J.H. Song, Piezoelectric nanogenerators based on zinc oxide nanowire arrays, Science 312 (5771) (2006) 242–246.
[24] C. Chang, H.V. Tran, J.B. Wang, Y.K. Fuh, L.W. Lin, Direct-write piezoelectric polymeric nanogenerator with high energy conversion efficiency, Nano Lett. 10 (2) (2010) 726–731.
[25] Y. Su, S. Li, R. Li, C. Dagdeviren, Splitting of neutral mechanical plane of conformal, multilayer piezoelectric mechanical energy harvester, Appl. Phys. Lett. 107 (2015) 041905.
[26] Z. Li, G. Zhu, R.S. Yang, A.C. Wang, Z.L. Wang, Muscle-driven *in vivo* nanogenerator, Adv. Mater. 22 (23) (2010) 2534–2537.
[27] G. Ciofani, A. Menciassi, Piezoelectric Nanomaterials for Biomedical Applications, Springer, New York, USA, 2012.
[28] G.-T. Hwang, H. Park, J.-H. Lee, S. Oh, K.-I. Park, M. Byun, H. Park, G. Ahn, C.K. Jeong, K. No, H. Kwon, S.-G. Lee, B. Joung, K.J. Lee, Self-powered cardiac pacemaker enabled by flexible single crystalline PMN-PT piezoelectric energy harvester, Adv. Mater. 26 (28) (2014) 4880–4887.
[29] H.S. Lee, J. Chung, G.-T. Hwang, C.K. Jeong, Y. Jung, J.-H. Kwak, H. Kang, M. Byun, W.D. Kim, S. Hur, S.-H. Oh, K.J. Lee, Flexible inorganic piezoelectric acoustic nanosensor for biomimetic artificial hair cells, Adv. Funct. Mater. 24 (44) (2014) 6914–6921.
[30] Q. Zhou, K.H. Lam, H. Zheng, W. Qiu, K.K. Shung, Piezoelectric single crystal ultrasonic transducers for biomedical applications, Prog. Mater. Sci. 66 (2014) 87–111.
[31] G.T. Hwang, Y. Kim, J. Lee, S. Oh, C. Jeong, D. Park, J. Ryu, H. Kwon, S. Lee, B. Joung, D. Kim, K. Lee, Self-powered deep brain stimulation via a flexible PIMNT energy harvester, Energy Environ. Sci. 8 (2015) 2677–2684.
[32] H. Zhang, X.S. Zhang, X. Cheng, Y. Liu, M. Han, X. Xue, S. Wang, F. Yang, S.A. Smitha, H. Zhang, Z. Xua, A flexible and implantable piezoelectric generator harvesting energy from the pulsation of ascending aorta: *in vitro* and *in vivo* studies, Nano Energy 12 (2015) 296–304.
[33] S. Xu, B.J. Hansen, Z.L. Wang, Piezoelectric-nanowire-enabled power source for driving wireless microelectronics, Nature Commun. 1 (2010) 93.
[34] W. Wu, S. Bai, M. Yuan, Y. Qin, Z.L. Wang, T. Jing, Lead zirconate titanate nanowire textile nanogenerator for wearable energy-harvesting and self-powered devices, ACS Nano 6 (7) (2012) 6231–6235.

[35] M. Lee, C.Y. Chen, S. Wang, S.N. Cha, Y.J. Park, J.M. Kim, L.J. Chou, Z.L. Wang, A hybrid piezoelectric structure for wearable nanogenerators, Adv. Mater. 24 (39) (2012) 1759–1764.

[36] L.M. Swallow, J.K. Luo, E. Siores, I. Patel, D. Dodds, A piezoelectric fibre composite based energy harvesting device for potential wearable applications, Smart Mater. Struct. 17 (2008) 025017.

[37] C.K. Jeong, J. Lee, S. Han, J. Ryu, G.-T. Hwang, D.Y. Park, J.H. Park, S.S. Lee, M. Byun, S.H. Ko, K.J. Lee, A hyper-stretchable elastic-composite energy harvester, Adv. Mater. 27 (18) (2015) 2866–2875.

[38] K. Tanaka, K. Suzuki, K. Nishizawa, T. Miki, K. Kato, Microstructure control and dielectric/piezoelectric properties of alkoxy-derived Ba(Ti, Zr)O_3 thin film, Japan. J. Appl. Phys. 44 (9B) (2005) 6885–6890.

[39] H. Maiwa, N. Iizawa, D. Togawa, T. Hayashi, W. Sakamoto, M. Yamada, S. Hirano, Electromechanical properties of Nd-doped $Bi_4Ti_3O_{12}$ films: A candidate for lead-free thin-film piezoelectrics, Appl. Phys. Lett. 82 (11) (2003) 1760–1762.

[40] A.L. Kholkin, K.G. Brooks, N. Setter, Electromechanical properties of $SrBi_2Ta_2O_9$ thin films, Appl. Phys. Lett. 71 (14) (1997) 2044–2046.

[41] Y. Nakashima, W. Sakamoto, H. Maiwa, T. Shimura, T. Yogo, Lead-free piezoelectric (K, Na)NbO_3 thin films derived from metal alkoxide precursors, Japan. J. Appl. Phys. 46 (14) (2007) L311–L313.

[42] Y. Saito, H. Takao, T. Tani, T. Nonoyama, K. Takatori, T. Homma, T. Nagaya, M. Nakamura, Lead-free piezoceramics, Nature 432 (2004) 84–87.

[43] C.K. Jeong, K.-I. Park, J. Ryu, G.-T. Hwang, K.J. Lee, Large-area and flexible lead-free nanocomposite generator using alkaline niobate particles and metal nanorod filler, Adv. Funct. Mater. 24 (18) (2014) 2620–2629.

[44] Y. Su, C. Dagdeviren, R. Li, Measured output voltages of piezoelectric devices depend on the resistance of voltmeter, Adv. Funct. Mater. 25 (33) (2015) 5320–5325.

[45] C. Dagdeviren, S.-W. Hwang, Y. Su, S. Kim, H. Cheng, O. Gur, R. Haney, F.G. Omenetto, Y. Huang, J.A. Rogers, Transient, biocompatible electronics and energy harvesters based on ZnO, Small 9 (20) (2013) 3398–3404.

[46] Y. Shi, C. Dagdeviren, C.F. Gao, J.A. Rogers, Y. Huang, An analytical model for skin modulus measurement via conformal piezoelectric systems, J. Appl. Mech. 82 (2015) 091007.

[47] J. Yuan, C. Dagdeviren, Y. Shi, Y. Ma, X. Feng, J.A. Rogers, Y. Huang, Computational models for the determination of depth-dependent mechanical properties of skin with a soft, flexible measurement device, Proc. R. Soc. Lond. Ser. A Math. Phys. Eng. Sci. (2016) under review.

[48] T. Starner, Human-powered wearable computing, IBM Syst. J. 35 (3&4) (1996) 618–629.

[49] Z.L. Wang, Toward self-powered nanosystems: From nanogenerators to nanopiezotronics, Adv. Funct. Mater. 18 (22) (2008) 3553–3567.

[50] C. Dagdeviren, Y. Su, P. Joe, R. Yona, Y. Liu, Y. Kim, Y. Huang, A. Damadoran, J. Xia, L. Martin, Y. Huang, J.A. Rogers, Conformable amplified lead zirconate titanate sensors with enhanced piezoelectric response for cutaneous pressure monitoring, Nature Commun. 5 (4496) (2014) 1–10.

[51] M. Meitl, Z. Zhu, V. Kumar, K.J. Lee, X. Feng, Y. Huang, I. Adesida, R. Nuzzo, J.A. Rogers, Transfer printing by kinetic control of adhesion to an elastomeric stamp, Nature Mater. 5 (2006) 33–38.

[52] A. Carlson, A.M. Bowen, Y. Huang, R.G. Nuzzo, J.A. Rogers, Transfer printing techniques for materials assembly and micro/nanodevice fabrication, Adv. Mater. 24 (39) (2012) 5284–5318.

[53] T.I. Kim, M.J. Kim, Y.H. Jung, H. Jang, C. Dagdeviren, H.A. Pao, S.J. Cho, A. Carlson, K.J. Yu, A. Ameen, H.-J. Chung, S.H. Jin, Z. Ma, J.A. Rogers, Thin film receiver materials for deterministic assembly by transfer printing, Chem. Mater. 26 (11) (2014) 3502–3507.

[54] M. Kang, J.H. Park, K.I. Lee, J.W. Cho, J. Bae, B.K. Ju, C.S. Lee, Fully flexible and transparent piezoelectric touch sensors based on ZnO nanowires and $BaTiO_3$-added SiO_2 capping layers, Phys. Status Solidi A 212 (9) (2015) 2005–20011.

[55] X. Wang, Q. Li, Z. Liu, J. Zhang, Z. Liu, R. Wang, Low temperature growth and properties of ZnO nanowire, Appl. Phys. Lett. 84 (24) (2004) 4941–4943.

[56] S. Xu, Y. Wei, M. Kirkham, J. Liu, W. Mai, D. Davidovic, R.L. Snyder, Z.L. Wang, Patterned growth of vertically aligned ZnO nanowire arrays on inorganic substrates at low temperature without catalyst, J. Am. Chem. Soc. 130 (45) (2008) 14958–14959.

[57] H.J. Xiang, J. Yang, J.G. Hou, Q. Zhu, Piezoelectricity in ZnO nanowires: a first-principles study, Appl. Phys. Lett. 89 (22) (2006) 223111.

[58] M.-H. Zhao, Z.-L. Wang, S.X. Mao, Piezoelectric characterization of individual zinc oxide nanobelt probed by piezoresponse force microscope, Nano Lett. 4 (4) (2004) 587–590.

[59] C. Li, W. Guo, Y. Kong, H. Gao, Size-dependent piezoelectricity in zinc oxide nanofilms from first-principles calculations, Appl. Phys. Lett. 90 (3) (2007) 033108.

[60] Y. Tan, J. Zhang, Y. Wu, C. Wang, V. Koval, B. Shi, H. Ye, R. McKinnon, G. Viola, H. Yan, Unfolding grain size effects in barium titanate ferroelectric ceramics, Sci. Rep. 5 (2015) 9953.

[61] Z.H. Lin, Y. Yang, J.M. Wu, Y. Liu, F. Zhang, Z.L. Wang, $BaTiO_3$ nanotubes-based flexible and transparent nanogenerators, J. Phys. Chem. Lett. 3 (23) (2012) 3599–3604.

[62] M. Akiyama, Y. Morofuji, T. Kamohara, K. Nishikubo, M. Tsubai, O. Fukuda, N. Ueno, Flexible piezoelectric pressure sensors using oriented aluminum nitride thin films prepared on polyethylene terephthalate films, J. Appl. Phys. 100 (11) (2006) 114318.

[63] X. Chen, S. Xu, X. Yao, W. Xu, Y. Shi, Potential measurement from a single lead zirconate titanate nanofiber using a manipulator, Appl. Phys. Lett. 94 (25) (2009) 253113.

[64] M. Fan, W. Hui, Z. Li, Z. Shen, H. Li, A. Jiang, Y. Chen, Fabrication and piezoresponse of electrospun ultra-fine $Pb(Zr_{0.3}, , , Ti_{0.7})O_3$ nanofibers, Microelectron. Eng. 98 (2012) 371–373.

[65] X. Feng, B.D. Yang, Y. Liu, Y. Wang, C. Dagdeviren, Z. Liu, A. Carlson, J. Li, Y. Huang, J.A. Rogers, Stretchable ferroelectric nanoribbons with wavy configurations on elastomeric substrates, ACS Nano 5 (4) (2011) 3326–3332.

[66] S. Troiler-McKinstry, F. Griggio, C. Yaeger, P. Jousse, D. Zhao, S.S. Bharadwaja, T.N. Jackson, S. Jesse, S.V. Kalinin, K. Wasa, Designing piezoelectric films for micro electromechanical systems, IEEE Trans. Ultrason. Ferroelectr. Freq. Control 58 (9) (2011) 1782–1792.

[67] F. Griggio, S. Jesse, A. Kumar, O. Ovchinnikov, H. Kim, T.N. Jackson, D. Damjanovic, S.V. Kalinin, S. Troiler-McKinstry, Substrate clamping effects on irreversible domain wall dynamics in lead zirconate titanate thin films, Phys. Rev. Lett. 108 (15) (2012) 157604.

[68] Z.H. Liu, C.T. Pan, L.W. Lin, J.C. Huang, Z.Y. Ou, Direct-write PVDF nonwoven fiber fabric energy harvesters via the hollow cylindrical near-field electrospinning process, Smart Mater. Struct. 23 (2014) 025003.

[69] N. Soin, T.H. Shah, S.C. Anand, J. Geng, W. Pornwannachai, P. Mandal, D. Reid, S. Sharma, R.L. Hadimani, D.V. Bayramol, E. Siores, Novel 3-D spacer all fibre piezoelectric textiles for energy harvesting applications, Energy Environ. Sci. 7 (5) (2014) 1670–1679.

[70] H. Kim, S.M. Kim, H. Son, H. Kim, B. Park, J. Ku, J.I. Sohn, K. Im, J.E. Jang, J.-J. Park, O. Kim, S. Cha, Y.J. Park, Enhancement of piezoelectricity via electrostatic effects on a textile platform, Energy Environ. Sci. 5 (10) (2012) 8932–8936.

[71] R. Steinhausen, T. Hauke, H. Beige, W. Watzka, U. Lange, D. Sporn, S. Gebhardt, A. Schönecker, Properties of fine scale piezoelectric PZT fibers with different Zr content, J. Eur. Ceram. Soc. 21 (10–11) (2001) 1459–1462.

[72] S. Xu, Y. Yeh, G. Poirier, M.C. McAlpine, R.A. Register, N. Yao, Flexible piezoelectric PMN-PT nanowire-based nanocomposite and device, Nano Lett. 13 (6) (2013) 2393–2398.

[73] K.-I. Park, S.B. Bae, S.H. Yang, H.I. Lee, K. Lee, S.J. Lee, Lead-free $BaTiO_3$ nanowires-based flexible nanocomposite generator, Nanoscale 6 (15) (2014) 8962–8968.

[74] S. Lee, S.-H. Bae, L. Lin, Y. Yang, C. Park, S.-W. Kim, S.N. Cha, H. Kim, Y.J. Park, Z.L. Wang, Super-flexible nanogenerator for energy harvesting from gentle wind and as an active deformation sensor, Adv. Mater. 23 (19) (2013) 2445–2449.

[75] Z.L. Wang, Piezopotential gated nanowire devices: Piezotronics and piezo-phototronics, Nano Today 5 (2010) 540–551.

[76] T.D. Nguyen, N. Deshmukh, J.M. Nagarah, T. Kramer, P.K. Purohit, M.J. Berry, M.C. McAlpine, Piezoelectric nanoribbons for monitoring cellular deformations, Nat. Nanotechnol. 7 (9) (2012) 587–593.

[77] Y. Ono, Q. Liu, M. Kobayashi, C.-K. Jen, A. Bluouin, A piezoelectric membrane sensor for biomedical monitoring, in: Proc. IEEE Ultrasonic Symp., 2006, pp. 800–803.

[78] H.-J. Tseng, W.-C. Tian, W.-J. Wu, Flexible PZT thin film tactile sensor for biomedical monitoring, Sensors 13 (5) (2013) 5478–5492.

[79] N. Ahmed, C. Dagdeviren, J.A. Rogers, P. Ferreira, Active polymeric composite membranes for localized actuation and sensing in microtransfer printing, J. Microelectromech. Syst. 24 (4) (2014) 1–13.

[80] J.-M. Breguet, W. Driesen, F. Kaegi, T. Cimprich, Applications of piezo-actuated micro-robots in micro-biology and material science, in: Proc. of the 2007 IEEE International Conference on Mechatronic and Automation, 2007, pp. 57–62.

[81] R. Rabe, J.-M. Breguet, P. Schwaller, S. Stauss, F.-J. Haug, J. Patscheider, J. Michler, Observation of fracture and plastic deformation during indentation and scratching insider the scanning electron microscope, Thin Solid Films 469–470 (2004) 206–213.